

Quantized Superfluid Vortex Filaments Induced by the Axial Flow Effect *

Hao Li(李浩)^{1,2,3}, Chong Liu(刘冲)^{1,2,3**}, Zhan-Ying Yang(杨战营)^{1,2,3}, Wen-Li Yang(杨文力)^{1,2,3,4}¹School of Physics, Northwest University, Xi'an 710127²Shaanxi Key Laboratory for Theoretical Physics Frontiers, Xi'an 710127³NSFC-SPTP Peng Huanwu Center for Fundamental Theory, Xi'an 710127⁴Institute of Modern Physics, Northwest University, Xi'an 710127

(Received 7 October 2019)

We report the quantized superfluid vortex filaments induced by the axial flow effect, which exhibit intriguing loop structures on helical vortexes. Such new vortex filaments correspond to a series of soliton excitations including the multipeak soliton, W-shaped soliton, and anti-dark soliton, which have no analogue when the axial flow effect is absent. In particular, we show that the vortex filaments induced by the multipeak soliton and W-shaped soliton arise from the dual action of bending and twisting of the vortex, while the vortex filament induced by the anti-dark soliton is caused only by the bending action, which is consistent with the case of the standard bright soliton. These results will deepen our understanding of breather-induced vortex filaments and will be helpful for controllable ring-like excitations on vortexes.

PACS: 03.75.Lm, 05.45.Yv, 67.25.dk

DOI: 10.1088/0256-307X/37/3/030302

Recently, research of quantum fluid has attracted considerable attention in many-particle systems^[1] and in optics.^[2] In either case, the motion of quantum fluid is most succinctly illustrated by vortex filament due to the fact that it consists of vorticity of infinite strength concentrated along the filament and gives an intuitive geometric interpretation of the evolution of the vorticity field. In particular, recent studies demonstrate that nonlinear excitations of vortex filaments are physically important since they are the main degrees of freedom remaining in a superfluid in the ultra low temperature regime. Such excitations are known as bright solitons^[3] and breathers.^[4,5] Importantly, the resulting vortex filaments exhibit intriguing loop structures which provide significant contributions to our understanding of quantum fluid and superfluid turbulence. Note that these results are based on the local induction approximation (LIA),^[6–8] which takes an assumption that the core radius of the vortex tube is infinitely small in comparison with the local radius of curvature.

However, the LIA becomes invalid as long as one considers the axial flow effect in vortex cores.^[9] Such an axial flow effect, which is different from the surrounding flow, plays a key role in tornadoes, bath-plug vortexes and trailing vortexes, and the size of the vortex tube cannot be ignored. This has been confirmed experimentally in Refs. [10,11], where the magnitude of the axial velocity near the core is substantial. Theoretically, with such an axial flow effect, the vortex filament induced by the two-pole soliton solution has been obtained.^[12] It has been shown that the axial flow effect only impacts the movement velocity of the vortex filament of two-pole soliton. In this Letter, we study the new quantized superfluid vortex

structures induced by the axial flow effect. In contrast to previous results, such new vortex filaments exhibit intriguing loop structures on helical vortexes, which correspond to a series of soliton excitations including the multipeak soliton, W-shaped soliton, and anti-dark soliton, which have no analogue in the case without the axial flow effect. In particular, we identify these vortex filaments by showing the distributions of curvature and torsion.

Hasimoto transformation and inverse map.—Considering the axial flow effect, the Biot–Savart equation, which gives the velocity at a point \mathbf{r} , can be reduced to the Moore–Saffman equation for the incompressible and inviscid fluid.^[9,13] Neglecting the non-local contribution along the vortex filament, a simpler fluid velocity equation is given by^[9]

$$\mathbf{r}_t = \alpha \mathbf{r}_s \times \mathbf{r}_{ss} + \beta \left(\mathbf{r}_{sss} + \frac{3}{2} \mathbf{r}_{ss} \times (\mathbf{r}_s \times \mathbf{r}_{ss}) \right), \quad (1)$$

where the subscripts indicate the partial differentiation with respect to the specified variables; $\mathbf{r}(s, t)$, as functions of arc length s and evolution time t , represents a point on the vortex filament; α depends on the circulation and effective vortex core radius; and β denotes the strength of axial flow effect. Repeating the Hasimoto transformation^[3] and making use of the Seret–Frenet equations given in Ref. [14], we have

$$\mathbf{r}_s = \mathbf{t}, \quad \mathbf{t}_s = \kappa \mathbf{n}, \quad \mathbf{n}_s = \tau \mathbf{b} - \kappa \mathbf{t}, \quad \mathbf{b}_s = -\tau \mathbf{n}, \quad (2)$$

where \mathbf{t} , \mathbf{n} , \mathbf{b} represent three mutually perpendicular unit vectors parallel to the tangent, the principal normal and the binormal directions respectively. Equation (1) can be reduced to the integrable Hirota

*Supported by the National Natural Science Foundation of China (Grant Nos. 11705145, 11875220, 11947301, 11434013 and 11425522), the Natural Science Basic Research Plan in Shaanxi Province of China (Grant No. 2018JQ1003), and the Major Basic Research Program of Natural Science of Shaanxi Province (Grant Nos. 2017KCT-12 and 2017ZDJC-32).

**Corresponding author. Email: chongliu@nwnu.edu.cn

© 2020 Chinese Physical Society and IOP Publishing Ltd

equation^[15]

$$i\psi_t - \alpha\left(\psi_{ss} + \frac{1}{2}|\psi|^2\psi\right) + i\beta\left(\frac{3}{2}|\psi|^2\psi_s + \psi_{sss}\right) = 0. \quad (3)$$

Here $\psi(s, t)$ is a complex function related with the local instantaneous parameters, i.e., curvature $\kappa(s, t)$ and torsion $\tau(s, t)$, by the transformation

$$\psi(s, t) = \kappa(\sigma, t)e^{i\int_0^s \tau(\sigma, t)ds}. \quad (4)$$

If $\beta = 0$, Eq. (3) reduces to the scalar cubic nonlinear Schrödinger equation (NLSE) of self-focusing type, and the resulting vortex structures induced by nonlinear waves have been studied.^[3–5,16] For the Hirota equation, the standard soliton induced vortex filament has been reported.^[12] The reconstruction of these excitations in the context of vortices can be achieved by the inverse map.^[17]

Vortex filaments with soliton modes induced by axial flow effect.—The axial flow effect introduces a series of new solitary vortex structures induced by multi-peak soliton, W-shaped soliton and anti-dark soliton, which have no analogue in the case that the axial flow effect is absent. We first consider the multi-peak soliton solution whose explicit expression is given by^[18]

$$\psi(s, t) = \left(1 + \frac{\Delta \cosh(\varphi + \delta) + \Theta \cos(\phi + \theta)}{\kappa_0 [\Omega \cosh(\varphi + \omega) + \Gamma \cos(\phi + \gamma)]}\right) \psi_0. \quad (5)$$

Here the plane wave background is given by $\psi_0 = \kappa_0 e^{i\theta}$ and $\theta = \tau_0 s + [\alpha(\tau_0^2 - \kappa_0^2/2) + \beta\tau_0(\tau_0^2 - 3/2\kappa_0^2)]t$. The parameters are defined as

$$\begin{aligned} \varphi &= \eta_i \xi, \quad \phi = \eta_r \xi, \quad \xi = s + vt, \\ v &= 2\beta(\kappa_0^2 + 2b^2 - 2\tau_1^2) - (\tau_1 + \tau_0)(4\tau_0\beta + \alpha), \\ \eta_r + i\eta_i &= \sqrt{\epsilon + i\epsilon'}, \quad \tau_1 = -\alpha/(2\beta) - \tau_0/2, \\ \epsilon &= \kappa_0^2 - b^2 + (\tau_0^2 - \tau_1^2), \quad \epsilon' = 2b(\tau_0 - \tau_1), \\ \Delta &= -4b\kappa_0\sqrt{\rho + \rho'}, \quad \Theta = 2b\sqrt{\chi^2 - (2\kappa_0^2 - \chi)^2}, \\ \Omega &= \rho + \rho', \quad \Gamma = -2\kappa_0(\eta_i + b), \\ \delta &= \operatorname{arctanh}(-i\chi_1/\chi_2), \\ \theta &= -\arctan[i(2\kappa_0^2 - \chi)/\chi], \\ \omega &= \gamma = 0, \end{aligned}$$

with $\rho = \epsilon + 2b^2 + \eta_i^2 + \eta_r^2$, $\rho' = \eta_r(2\tau_0 - \tau_1) + 2\eta_i b$, $\chi_1 = \eta_r + (\tau_0 - \tau_1/2)$, $\chi_2 = b + \eta_i$ and $\chi = \chi_1^2 + \chi_2^2 + \kappa_0^2$.

The plane wave background ψ_0 corresponds to a trivial uniform helical vortex filament with κ_0 and τ_0 describing the curvature and torsion respectively. In contrast, the multi-peak soliton (5), which describes the motion of a nontrivial helical vortex filament influenced by localized periodic disturbance, exhibits more interesting and complex behavior.

Figures 1(a) and 1(c) show the temporal evolutions of curvature and torsion on the (ξ, t) plane (here $\xi = s + vt$ denotes the moving frame on the group velocity) under the condition $\alpha = 1$, $\beta = 3$, $\kappa_0 = 1$,

$\tau_0 = -\alpha/(8\beta)$ and $b = 0.4$. As is expected, the curvature and torsion remain stable as t increases. We also show the surface plot of the curvature κ and torsion τ at $t = 0$ in Figs. 1(b) and 1(d). It is clear that both curvature and torsion are localized forms with the same period.

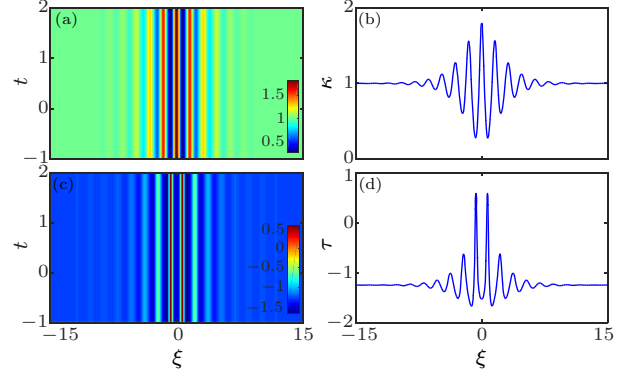


Fig. 1. Temporal evolutions of curvature $\kappa(\xi, t)$ (a) and torsion $\tau(\xi, t)$ (c), given by Eqs. (4) and (5), corresponding to a multi-peak soliton. [(b), (d)] Variations of $\kappa(\xi, t)$ and $\tau(\xi, t)$ at $t = 0$. The other parameters are $\alpha = 1$, $\beta = 3$, $\kappa_0 = 1$, $\tau_0 = -\alpha/(8\beta)$ and $b = 0.4$.

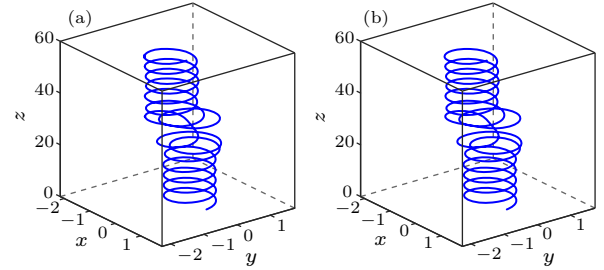


Fig. 2. Configuration of vortex filaments of multi-peak soliton at different times: (a) $t = 0$, (b) $t = 1$. The other parameters are the same as those in Fig. 1.

The corresponding vortex structure induced by the multi-peak soliton is shown in Fig. 2. One can see clearly that such a nonlinear soliton excitation admits a collected multi-loop structure with different sizes on a uniform helical filament. As t increases, this vortex structure remains unchanged, which inherits the property of the soliton.

Next, we concentrate our attention on the motion of a locally but nonperiodically perturbed helical vortex filament corresponding to the soliton excitations. In this case, the torsion of the uniform helical filament plays an important role and should be a constant $\tau_0 = -\alpha/(3\beta)$. That is to say, $\tau_1 = \tau_0$ in Eq. (5). Specially, the soliton excitation exists when $\eta_r = 0$, i.e., $b > \kappa_0$. The explicit expression reads

$$\psi_w = \left[\frac{2\eta_i^2}{\kappa_0 b \cosh(\eta_i \xi) - \kappa_0^2} - 1 \right] \psi_0, \quad (6)$$

where $\eta_i = \sqrt{b^2 - \kappa_0^2}$ and $\xi = s + v_1 t$ with $v_1 = 2\tau_0\alpha - \beta(\kappa_0^2 + 2b^2 - 6\tau_0^2)/2$. This soliton, with one peak and two valleys, is the so called W-shaped soliton.^[19–21]

The variations of curvature and torsion of the vor-

tex filament induced by W-shaped soliton are shown in Figs. 3(a) and 3(c), which remain unchanged as t increases. Here the parameters are set as $\alpha = 1$, $\beta = 3$, $\kappa_0 = 1$, and $b = 1.3$. The specific envelope of curvature and torsion at $t = -0.1$ are shown in Figs. 3(b) and 3(d), respectively. We find that the torsion has striking extreme points at the place where the curvature is minimal, which leads to the severe twisting of the vortex filament. We also point out that the two extreme points of the torsion have opposite signs, which means the corresponding vortex structure twist in opposite directions around the point of maximum curvature. In Fig. 4(a), we show this solution at different times $t = -0.1$, $t = -0.06$ and $t = -0.01$. It is clear that the solution admits a loop structure on a uniform helical filament due to the dual action of bending and twisting of the vortex.

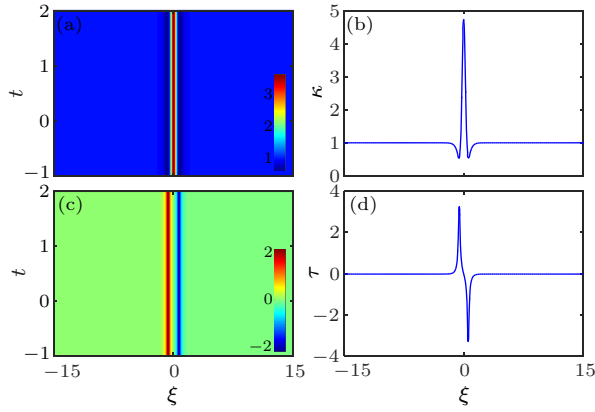


Fig. 3. Temporal evolutions of curvature $\kappa(\xi, t)$ (a) and torsion $\tau(\xi, t)$ (c) corresponding to a W-shaped soliton. [(b), (d)] Variations of $\kappa(\xi, t)$ and $\tau(\xi, t)$ at $t = -0.1$. The other parameters are $\alpha = 1$, $\beta = 3$, $\kappa_0 = 1$, $b = 1.3$, $\tau_0 = -\alpha/(3\beta)$.

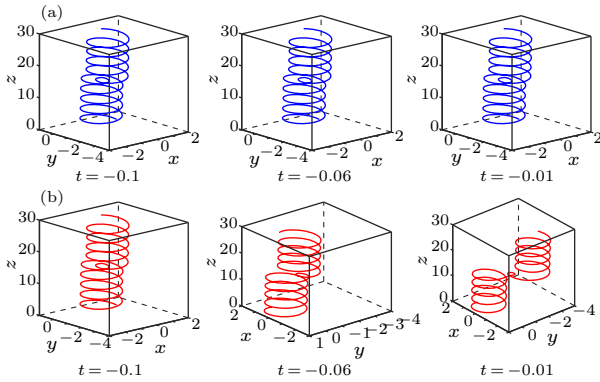


Fig. 4. Configuration of vortex filaments of (a) W-shaped soliton and (b) Kuznetsov–Ma breather at different times $t = -0.1$, $t = -0.06$, $t = -0.01$, $\tau_0 = -\alpha/(3\beta)$ for W-shaped soliton and $\tau_0 = -0.1$ for Kuznetsov–Ma breather.

Note that the W-shaped soliton is a special case of the Kuznetsov–Ma breather,^[18,22] where the growth-decay cycle tends to zero. In Fig. 4(b), we use the same initial state as Fig. 4(a) at $t = -0.1$ besides the $\tau_0 = -0.1$ and present the motion of the Kuznetsov–Ma breather induced vortex filament. A notable dif-

ference is that the size of loop structure induced by the Kuznetsov–Ma breather changes gradually as t increases and this process will emerge periodically, while the W-shaped soliton induced loop structure remains unchanged over time. The reason for this phenomenon is that when $\tau_0 \neq -\alpha/(3\beta)$, the soliton solution will be converted to an unstable ‘breathing’ mode. Therefore we point out that the vortex structures which start from the same locally perturbed helical filament may be absolutely different due to the introduction of axial flow effect.

In addition to W-shaped soliton, the motion of a locally perturbed helical vortex filament can also be described by the anti-dark soliton which is first shown in the NLS system with third-order dispersion.^[23] There exists a slight phase shift with W-shaped soliton and its explicit expression for Eq. (3) is given by

$$\psi_a = \left[1 + \frac{2\eta_i^2}{\kappa_0 b \cosh(2\eta_i \xi + \mu) + \kappa_0^2} \right] \psi_0, \quad (7)$$

where $\mu = \arctan(-\eta_i/b)$ and $\xi = s + v_2 t$ with $v_2 = -\alpha^2/3\beta - \beta(\kappa_0^2 + 2b^2)/2$. In the limit of $\kappa_0 \rightarrow 0$, the anti-dark soliton can be transformed into the standard bright soliton (BS) on the vanishing background as follows:

$$\psi_b = 2b \operatorname{sech}(2\eta_i \xi + \mu_0) \exp[i(\tau_0 s + \omega t)]. \quad (8)$$

Here μ_0 is an arbitrary constant. Actually, the anti-dark soliton can be seen as a bright soliton on a non-vanishing background.

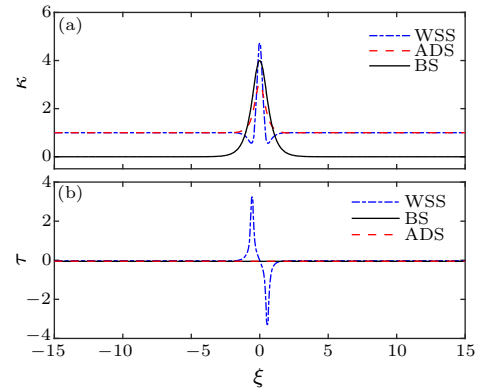


Fig. 5. Variation of curvature $\kappa(\xi, t)$ (a) and torsion $\tau(\xi, t)$ (b) corresponding to the W-shaped soliton, anti-dark soliton and bright soliton at a fixed time $t = -0.1$. The other parameters are $\alpha = 1$, $\beta = 3$, $\kappa_0 = 1$, $\tau_0 = -\alpha/(3\beta)$ and $b = 2$.

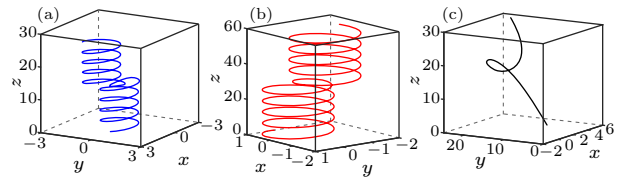


Fig. 6. Configuration of vortex filaments of (a) W-shaped soliton, (b) anti-dark soliton and (c) bright soliton at a fixed time $t = -0.1$. The other parameters are the same as those in Fig. 5.

Figures 5(a) and 5(b) show the variations of curvature and torsion of the vortex filaments induced by

W-shaped soliton, anti-dark soliton and bright soliton, respectively, under the condition $\alpha = 1$, $\beta = 3$, $\kappa_0 = 1$, $\tau_0 = -\alpha/(3\beta)$, $b = 2$ and $t = -0.1$. Remarkably, for the vortex structures corresponding to anti-dark soliton and bright soliton, the perturbation only increases the local curvature relative to the uniform helical filament background and has no contribution to the torsion, which is different from that of W-shaped soliton.

The vortex structures induced by W-shaped soliton, anti-dark soliton and bright soliton are presented in Figs. 6(a)–6(c), respectively. One can clearly know from the figure that the torsion of the latter two soliton is a constant, which is different from the former. This means that the twist direction of the vortex structure induced by anti-dark soliton and bright soliton remains unchanged, and the corresponding loop structures are only influenced by the bending action of curvature. The major difference between the latter two vortex structures is that the anti-dark soliton induces the loop structure on a uniform helical filament, while the bright soliton on a vortex line with zero curvature.

In summary, we have investigated new quantized superfluid vortex filaments induced by the multipeak soliton, W-shaped soliton and anti-dark soliton, which are affected by the axial flow effect. We present two types of loop structures: one arises from the dual action of bending and twisting of the vortex, which is induced by the multipeak soliton and W-shaped soliton; the other is generated only from the bending action of curvature corresponding to anti-dark soliton and bright soliton. Meanwhile, We compare the vortex filaments induced by W-shaped soliton and Kuznetsov–Ma breather, and demonstrate that the vortex structures which start from the same locally perturbed helical filament may be absolutely different due to the

axial flow effect.

References

- [1] Barenghi C F and Parker N G 2016 *A Primer on Quantum Fluids* (Berlin: Springer)
- [2] Carusotto I and Ciuti C 2013 *Rev. Mod. Phys.* **85** 299
- [3] Hasimoto H 1972 *J. Fluid Mech.* **51** 477
- [4] Salman H 2013 *Phys. Rev. Lett.* **111** 165301
- [5] Salman H 2014 *J. Phys.: Conf. Ser.* **544** 012005
- [6] Arms R J and Hama F R 1965 *Phys. Fluids* **8** 553
- [7] Da Rios L S 1906 *Rendiconti del Circolo Matematico di Palermo* **22** 117
- [8] Betchov R 1965 *J. Fluid Mech.* **22** 471
- [9] Fukumoto Y and Miyazaki T 1991 *J. Fluid Mech.* **222** 369
- [10] Maxworthy T, Hopfinger E J and Redekopp L G 1985 *J. Fluid Mech.* **151** 141
- [11] Maxworthy T, Mory M and Hopfinger E J 1983 *AGARD Conference Proceedings* **342** paper 29
- [12] Demontis F, Ortenzi G and Van Der Mee C 2015 *Physica D* **313** 61
- [13] Moore D W and Saffman P G 1972 *Philos. Trans. Roy. Soc. London Ser. A* **272** 403
- [14] Pismen L M 1999 *Vortices in Nonlinear Fields* (Oxford: Clarendon)
- [15] Hirota R 1973 *J. Math. Phys.* **14** 805
- [16] Li H, Liu C, Zhao W, Yang Z Y and Yang W L 2019 [arXiv:1905.07878](https://arxiv.org/abs/1905.07878) [nlin.PS]
- [17] Shah R 2015 *Rogue Waves on a Vortex Filament* (Oxford: Oxford University Press)
- [18] Liu C, Yang Z Y, Zhao L C, Duan L, Yang G Y and Yang W L 2016 *Phys. Rev. E* **94** 042221
- [19] Li Z H, Li L, Tian H P and Zhou G S 2000 *Phys. Rev. Lett.* **84** 4096
- [20] Zhao L C, Li S C and Ling L M 2014 *Phys. Rev. E* **89** 023210
- [21] Liu C, Yang Z Y, Zhao L C and Yang W L 2015 *Phys. Rev. E* **91** 022904
- [22] Kuznetsov E 1977 *Sov. Phys. Dokl.* **22** 507
Ma Y C 1979 *Stud. Appl. Math.* **60** 43
- [23] Kivshar Y S 1991 *Phys. Rev. A* **43** 1677(R)
Kivshar Y S and Afanasjev V V 1991 *Phys. Rev. A* **44** R1446